

PAIRWISE QUASAR CORRELATIONS AND BELL'S INEQUALITY

ERIC STEINBRING¹

Revised, December 11, 2018

ABSTRACT

Viewing two sources at sufficient distance and angular separation can assure, by light-travel-time arguments, the acausality of their emitted photons. Using these photons to set apparatus parameters in a laboratory-based quantum-mechanical experiment could ensure those settings are independent too, allowing a decisive, loophole-free test of Bell's inequality. Quasars are a natural choice for such objects, as they are visible up to high redshift and pointlike. Yet applying them at the ultimate limit of the technique involves simultaneous flux measurements in opposite directions on the sky. This presents a challenge to proving randomness against either noise or an underlying signal. By means of a “virtual test” and simple signal-to-noise calculations, bias in ground-based optical photometry while performing an Earth-wide test is explored, imposed by fluctuating sky conditions and instrumental errors including photometric zeropoints. Analysis for one useful dataset from the Gemini Observatory telescopes is presented, using over 14 years of archival images obtained with their Multi-Object Spectrograph (GMOS) instrument twins, serendipitously sampling thousands of quasars up to 180° apart. These do show correlation: an average pairwise broadband optical flux difference intriguingly consistent with the form of Bell's inequality. That is interesting in itself, if not also a harm to experimental setting independence; some considerations for future observations are discussed.

Subject headings: quasars, cosmology, techniques, site testing

1. INTRODUCTION

That quantum mechanics (QM) must be incomplete, allowing outcomes requiring either super-luminal signals or “hidden” unmeasured variables was famously contended by Einstein, Podolsky and Rosen (1935). Bell (1964) showed that correlations in a QM experiment could allow tests against such unsensed influences. Experiments routinely find QM is correct, and have tightly and simultaneously restricted necessary conditions on measurements (e.g. Rosenfeld et al. 2017 and references therein) but not excluded a final possibility, by closing the so-called “freedom-of-choice” loophole and fully eliminating experimenter interaction in the result. One promising route is to set experimental parameters via photons from astronomical sources (Friedman, Kaiser and Gallicchio 2013; Gallicchio, Friedman and Kaiser 2014), requiring that any interference between two settings have been orchestrated between distant sources and the Earth-based observer. Proof-of-concept QM tests using stars within the Milky Way were already achieved by Handsteiner et al. (2017) and Li et al. (2018) forcing any “collusion” in the outcome back hundreds of years. And a recent exciting development was the extension to quasars (Rauch et al. 2018): the combination of high redshift with large angular separation on the sky can place these entirely outside each others' light cone; for separations of 180° this occurs when both sources have $z \geq 3.65$. The independence of settings triggered by those photons is unspoiled by their communication, and absent correlated errors corrupting that signal prior to detection, forces any unexplained coincidence to be the result of unexpected synchronization between sources. Otherwise, the foundations of QM

would indeed be in question.

The quasar-based QM experiment performed by Rauch et al. (2018) follows the methodology of Clauser et al. (1969) where an entangled pair of photons emitted from a central source are split between two optical arms and their polarizations are detected at receivers. While those entangled photons are in flight, a switching mechanism at each receiver (also co-located with a telescope) selects randomly between two potential polarization measurements. In these first quasar test runs that switch was set by the colour of the most recently detected photon, using bright pairs viewed separately via two 4-m class telescopes from Observatorio del Roque de los Muchachos on La Palma. One quasar pair had $z = 0.268$ and 3.911, with another at 0.964 and 3.911. Their fluxes were sufficient to allow large sampling losses: a relative polarization measurement was retained only if both quasar photons arrived during the microseconds while the entangled photons were in flight. Neither the colours of the two quasars nor background noise against which they were detected (notably sky brightness) were seen to be correlated during the runs, which lasted between 12 and 17 minutes. This experiment strongly upheld QM, while safely ruling out collusion between polarization settings.

Can a QM experiment utilizing antipodal, and truly acausal, quasar pairs be performed? The primary hurdle to one as described above is that such sightlines are effectively impossible from any single location on the Earth. A spaceborne mission with sufficient field of regard might do so, possibly even via direct photon-counting of γ -rays or X-rays. It is notable, however, that despite decades of optical variability studies (e.g. MacLeod et al. 2010) and extensive reverberation mapping having established the characteristic sizes of AGN disks on the order of light days across (Mudd et al. 2018), no simultane-

¹ National Research Council Canada, Herzberg Astronomy and Astrophysics, Victoria, BC V9E 2E7, Canada

ous monitoring campaign of such sources outside each others' horizon is so far reported in the literature, at any wavelength. The difficulty from the ground is, of course, hindrance by the Earth. Radio telescopes do not gain a benefit in this regard, as dish elevations are well above the local horizon, regardless of Sun position. From the nightside, optical/near-infrared observatories are restricted to separations less than 90° from any single site, hemmed below two airmasses. At minimum, this incurs twice the zenith extinction for both, even under photometric skies, with similarly degraded seeing. Darkness reaches only ~ 21 mag arcsec $^{-2}$ in the visible, which is relevant for two well-separated quasars, both typically fainter. What must be overcome is colour-discrimination of those, viewed independently and simultaneously from *opposite hemispheres*. This is undemonstrated, which although not obviating previous QM experiments, does set a bar for an irrefutable ground-based one.

Practical aspects of connecting the sites aside, at least one useful dataset to probe is available for Gemini: on Maunakea in Hawaii (19.82°N , 155.47°W , 4213 m) and on Cerro Pachon in Chile (30.24°S , 70.74°W , 2722 m), that when each viewing a target near zenith, places those 95.5° apart on the sky. These 8-m class telescopes have operated near-identical optical imagers continuously for over 15 years, and a public archive eases aggregation of many serendipitous observations. Although such data do not, in themselves, constitute a QM experiment, they may provide a baseline for devising a future one: at over 10600 km apart across the Pacific Ocean, no collusion is possible on timescales less than this distance over the speed of light or $l/c \approx 0.04$ seconds, which in the rest-frame at $z = 4$ corresponds to 0.2 seconds.

The next section outlines how limitations on simultaneous photometry of quasars at large angular separation restricts their best expected relative signal-to-noise ratio, whether exploitable in a Bell theorem test to mimic QM or not. The motivation is to determine if any underlying signal may remain. To look for a potential one, a “virtual test” is suggested with sources chosen in a randomized way to avoid bias and sky conditions sampled sufficiently to remove their influence. Following that, the available Gemini dataset is described, which consists of g , r , i , z photometry for thousands of quasars with redshifts $0.1 < z < 6$, sensitive down to 23 mag. The total sample comprises roughly 2 million observational pairs, which in their aggregate (0.25-magnitude $1\text{-}\sigma$ uncertainty within 6-degree-wide sampling bins) is just sufficient to show a difference in brightness relative to object separation matching Bell’s inequality. Discussion follows on the prospects in the era of 30-m telescopes, and reaching the necessary photometric accuracy to exclude local noise sources in closing the last observational loophole.

2. EXPECTED SIGNAL-TO-NOISE RATIO

The intent is to quantify a correlated lack of randomness in external source fluxes relative to local noise, and so a general description of a QM experiment is sufficient to illustrate how this might be connected to setting independence in a Bell-theorem test, even if that were ideal. Generically, quantum theory demands that entangled photon pairs must be found in opposite polarization states; if one is found with horizontal polarization, the state of its entangled twin will always be found verti-

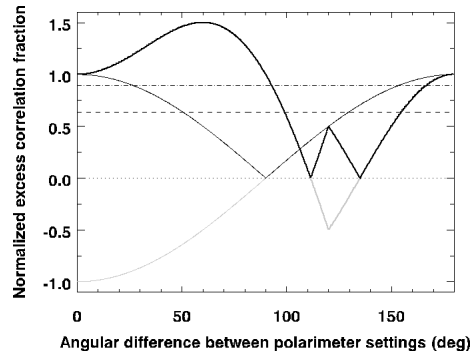


FIG. 1.— Normalized fraction of correlated photon polarizations with waveplate-angle difference in an idealized optical QM experiment described in the text; here, the absolute value is taken (thin black curve). Bell’s theorem (thick black curve) shows that the QM prediction for correlations would be in excess of what could possibly be explained through hidden, unmeasured variables; those averages are indicated by dot-dashed and dashed lines respectively, against no correlation at all (dotted).

cal. (In the original theoretic treatment, these were the spin states of entangled electrons: up or down.) Importantly, any real experiment cannot measure both states in one direction simultaneously, as this requires a setting change. For example, polarimetry necessitates a discriminator, such as a polarizer or the rotation of a waveplate. A choice must be made as to which polarization angle (or arm) to sample. Detecting the state of one entangled photon instantly collapses the wavefunction of both subject to shared uncertainty, demanding for the other a probability density which depends on the angle between waveplate settings. Those states must be anti-correlated when co-incident (there are exactly two possibilities) and thus in order to preserve equal average probabilities of both states, this implies no net correlation at 90° difference, and a functional form for normalized correlation of $-\cos\phi$, where ϕ is in degrees (see Figure 1). But the experimenter’s ability to freely choose settings - and so not be complicit in the outcome - cannot be assumed, and when not this takes on the form (Bell 1964):

$$P(\phi) = |\cos 2\phi - \cos \phi| + \cos \phi, \quad (1)$$

which exceeds unity for all lesser angles. Finding that unequal or “excess” correlation, above equality and beyond what truly random sampling predicts, would reveal a fundamental fault in QM.

In a true loophole-free QM test, the switching photons effectively operate the apparatus, automating setting changes photon-by-photon between settings by predefined selection criteria. Any criterion can only ever be a relative flux measurement over some suitably defined passband and time period. So an issue would arise if the colour of sensed switching photons at the telescope were dominated by local noise. Either the sources or switching mechanisms could retain hidden correlation. Admittedly, unless strong, that may not predict the colour of the next photon to arrive, so not exploitable to mimic QM behaviour. But even if weak, equation 1 is logically one functional form of correlation to look for, which is immediately connected to the relative noise between telescopes. That correlation cannot be avoided from the ground: the observational errors such as seeing, sky background and extinction are well known to depend on air-mass, and if not removed perfectly inject some cosine

dependence with viewing angle θ . Imagine that, instead of angular polarizer difference ϕ , source correlation is exhibited by their angular separation ($\phi = \theta$). Correlation might then be impossible to fully exclude.

The requirement on how uncorrelated sources must be to avoid this particular bias, if real, can still follow by working backwards from the needs of setting independence: finding sufficient flux difference beyond observational noise for any two randomly-selected sources to be confident that switching based on those was *not* random. Although quasars are known to fluctuate on timescales of days to many years, and likely do so on timescales as short as the QM experiment, as a group they have well-studied optical brightness distributions. So if any two quasars were sampled in a perfectly unbiased way from a distribution of width ω magnitudes, they should, over a long-term average, have a maximal difference between them, if amplified by equation 1, of

$$\Delta S = 2\omega P, \quad (2)$$

in magnitudes. The signal amounts to an excess relative to flatness with separation angle, and so the absolute value of this can be taken. And thus the problem becomes one of determining how many quasars to sample at random, for how long, and how accurately to overcome uncertainty in flux measurements, which at minimum will be restricted by the instrumental error in relative flux difference, and from the ground is likely further impacted by variation of sky brightness, seeing, and atmospheric extinction on similar timescales.

Consider identical instruments at two sites with a geographic separation of 90 degrees, that is, two sources viewed simultaneously at zenith would be separated by 90 degrees. (This is essentially the case for Gemini North and South: 95.5 degrees apart.) Under clear skies, atmospheric extinction increases linearly with airmass, inversely with zenith distance ($1/Z$), so for any target under an airmass of 2, the difference between it any other θ degrees away, is at its extreme

$$E(\theta) = \left| 2 - \frac{\sqrt{2}}{\cos(\theta/2)} \right|, \quad (3)$$

or

$$\Delta A = \alpha E, \quad (4)$$

where α is half the median extinction in magnitudes. A similar relationship can be found for sky brightness,

$$\Delta B = \beta E, \quad (5)$$

and image quality

$$\Delta Q = \gamma E, \quad (6)$$

where β is in units of mag arcsec^{-2} , and γ is in arcseconds. The functional form of E has a zenith distance more like the standard expression of Kasten (1965), which is $Z = \cos(\theta/2) + 0.150 \times (93.885 - \theta/2)^{-1.253}$, and for seeing ($E = E_Q$) is perhaps better modeled with a weaker $Z^{0.6}$ power. And while one site is still enjoying better weather, the other might continue imaging only under 80%-ile conditions, a relative factor $2.5\times$ poorer than the median. Those limits are shown in Figure 2, represented by a thin line and a dot-dashed line respectively. Later it will be shown that for Gemini $\alpha \approx 0.25$ mag, $\beta \approx 0.40$ mag arcsec^{-2} , and $\gamma \approx 0.38$ arcsec; so those

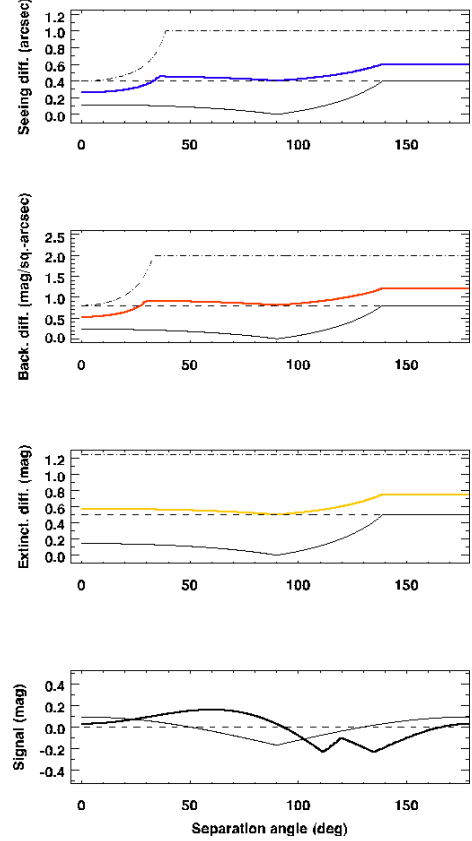


FIG. 2.— Model differences in seeing (blue), and extinction (yellow) between any two positions on the sky up to 180 degrees apart, viewed from two different sites, here plotted for Gemini. Instantaneous lower and upper limits (dot-dashed) are indicated, giving means for coincident observations (thick curves) and long-term medians for combining views from each single site (dashed lines). Below is an expected difference in flux of two quasars selected at random from a brightness distribution of width 1.0 mag, if their fluxes were correlated as per Bell's theorem, and reaching a mean of $S/N = 3$ as per equation 7 (thick black curve).

values are adopted in Figure 2. Their averages are shown as thick curves.

The signal-to-noise ratio of detectable enhancement in flux differences over observational noise for n samples thus has the form

$$S/N \approx \frac{2\omega P}{(\alpha E + \beta \gamma^2 E E_Q^2 + \delta)/\sqrt{n} + \zeta}, \quad (7)$$

where δ is the photometric uncertainty and ζ is the band-pass zeropoint error, both in magnitudes. Note that, as they are maximal, $\Delta A + \Delta B + \Delta Q$ are not added in quadrature, and fall off as the square-root of the number of samples, as does photometric uncertainty. Binning the data can enhance S/N only until it reaches the zeropoint accuracy. So the maximum detectable effect for any randomly selected pair, even in a space-based observation, is limited by the peak of P and calibration error to be

$$S/N \leq 3\omega/\zeta. \quad (8)$$

The width of the quasar-brightness distribution in the optical is about $\omega = 1.0$ magnitude, and photometric accuracy limited by zeropoint knowledge to typically 2%, thus $S/N \leq 150$. Relative measurements for a given angle should still be dominated by their shared photometric uncertainty until sufficient samples beat that down below

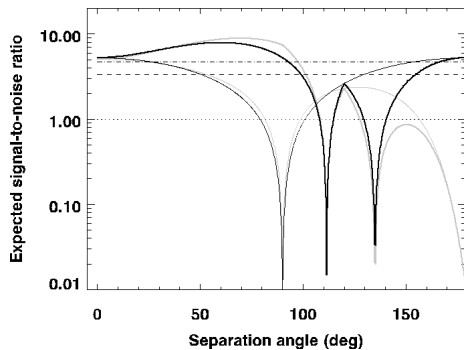


FIG. 3.— Expected signal-to-noise ratios: grey curves (thick for Bell’s theorem) for simultaneous single exposures with minimal error; black curves assume long-term sampling and $n = 3000$. Horizontal dashed and dot-dashed (Bell’s theorem) are averages over all angles.

twice the zeropoint error, which for 0.25 mag occurs at $n = 10$. For reference, 10 Gemini FoVs (5 arcmin across) spans roughly one degree. Averaged over the whole sky, a detection minimum, for $S/N = 3$, is shown in Figure 2. The form of this curve suggests one further constraint: the peak at $\theta = 120^\circ$ is 23.4 degrees across, not critically spanned by less than three samples; two per side would be maximal bins about 6 degrees wide.

A proportional relationship between sampling and detectable signal is further illustrated in Figure 3. For many samples in a long-term average, $E_Q = E = 1$, which implies that (sampled over all angles) it slowly grows over $S/N = 3$ by $n = 3000$ (3.6 for 10000) with photometric uncertainty fixed at 0.25 mag. This is indicated by the black curves, which suggests that to achieve similar constraints either a single pair with minimum observational noise or a larger, noisier (but binned) sample across the full sky may present comparable ways to detect the influence of P . It is the latter method which is adopted here: obtaining good relative photometry for an unbiased sample of quasars over many years, and looking for a relative dependence with angular separation.

3. SAMPLE

Archival Gemini Multi-Object Spectrograph (GMOS) images were searched for all instances of a known quasar falling into the field, starting from the beginning of regular GMOS operations to the beginning of 2016, spanning 14.5 years. A difficulty with a direct search is that the file header information will include a target name selected by the observer, which may not necessarily correspond to any catalog. Also, this would exclude cases where an object happened to fall on the detector during the observation of another, defined target. So instead the Million Quasars Catalog (MILLIQUAS), Version 4.8 of 22 June 2016 was cross-correlated with the full Canadian Astronomy Data Center (CADC) archive of science frames obtained with GMOS North and South. The MILLIQUAS is a compendium of published catalogs, primarily the Sloan Digital Sky Survey (SDSS) providing a redshift plus optical magnitudes (Blue: B , V or g ; and Red: r or i) for each object. No restriction on type was made, including gravitational lenses, but the likelihood of misidentifications is considered small.

The GMOS field of view (FoV) is approximately 5×5 arcmin², with 0.075 arcsec pixels. Using the Common Archive Observation Model (CAOM) Table Ac-

cess Protocol (TAP) web service and custom Python scripts, a search within a 5 arcmin radius for each object was conducted, which produced 28374 cases where an $0.1 < z < 6$ object was within a GMOS g , r , i , or z field, through the full range of right ascension, and between -79° and $+82^\circ$ declination; deleting those corrupted or otherwise unusable yielding 20514 objects (g : 4691, r : 6709, i : 6776, z : 2338), and a typical exposure time of about 150 seconds. Gemini records each science frame within clear-sky-fraction bins from CC20 (best 20%-ile) to CCAny (all conditions). This represents 11483 unique (although potentially repeated) objects having a mean redshift of 1.48, no noticeable dependence on sky position, and obtained under all conditions under which the telescopes were operational.

Finally, a selection was made to ensure good data quality for each observation. Every object frame was searched for a comparison star from the Fourth U.S. Naval Observatory CCD Astrograph Survey (UCAC4) to serve as a photometric calibration, with published SDSS r magnitude. There were 16774 frames that had such a suitable, unsaturated star. This also provided for each an image quality criterion; image Point-Spread Function (PSF) Full-Width-at-Half Maximum (FWHM) was extracted for each star. The FWHM of the object (also confirmed to be unsaturated) was checked against this; in just a few cases where it occurred, the smaller of the two was taken. A lower FWHM limit of 0.20 arcsec was applied to ensure that only real images were obtained, without artifacts, and so it reflects seeing conditions. After this, only 9317 objects remained after culling for cloud-cover conditions better than CC80, or usable, with less than 2 magnitudes of extinction.

4. PHOTOMETRY

Synthetic aperture photometry was carried out on the full sample, both objects and comparison stars, using a 4 arcsec diameter aperture throughout. Roughly 20 arcsec² postage stamps sections were downloaded from the database. The positional accuracy of the frames was found by inspection to not always be better than 2 arcseconds. During the FWHM measuring step, a centroiding algorithm located the central pixel position and then sub-pixel shifted the aperture prior to obtaining the flux. Median sky backgrounds for each frame were subtracted after applying the appropriate detector gains and filter zeropoints, as published on the Gemini webpages. The detectors, and their configurations at the focal plane changed at certain times, either 4 or 6 chips across the FoV with separate amplifiers and gaps between them, and each detector has a slightly different amplifier response. On average these are 28.11, 28.31, 28.16 and 27.17 mag in g , r , i and z , which fluctuated over that time with deviations of 0.12, 0.02, 0.12 and 0.22 mag respectively.

All resultant photometry was corrected for atmospheric extinction using the calibration stars, where each of those was relative to its UCAC4 r magnitude and a mean filter correction. This was calculated using the 237 observations with complete photometry in MILLIQUAS catalogued B , V , r and i magnitudes, which allows the calculation of a mean sample colour shift to B , V , r , and i of 0.84, 0.49, 0.34, and 0.19 mag; g was interpolated as 0.66 mag and z extrapolated to 0.18 mag. Of these, 124 were cases of objects included in the UCAC4 catalog,

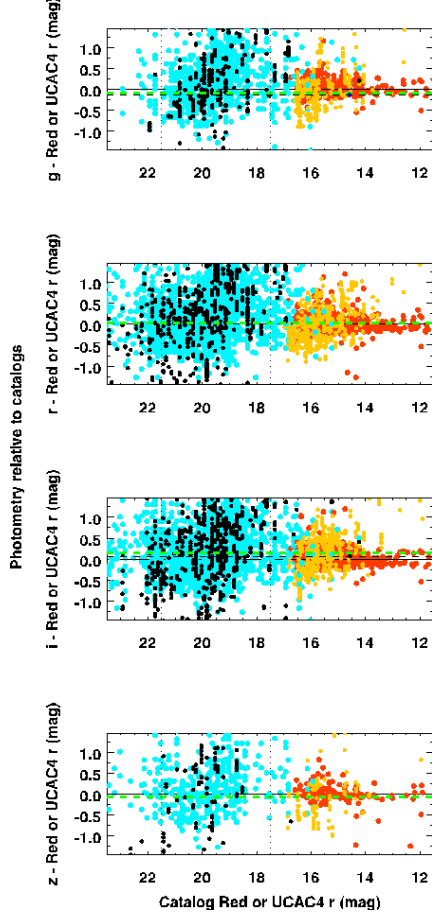


FIG. 4.— Differences of observed from catalog magnitudes for objects (black) and comparisons (yellow) in the four filters studied. For reference, the relative colours of those against MILLIQUAS Blue (light blue) and UCAC4 i (red) are also shown; mean comparison colours (dashed green) are neutral, as are the objects (dashed black). Those last have been limited to within magnitude cutoffs (vertical dotted lines), serving to avoid any colour bias in the sample; if perfectly Gaussian these would be zero.

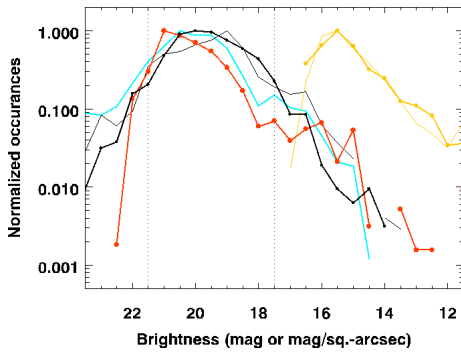


FIG. 5.— Histograms of sky background (red curve), object (black), and comparison star (yellow) magnitudes, normalized to their peak occurrences. Observed magnitudes are comparable to their catalog MILLIQUAS Blue (blue curve) and Red (thin black) values as are comparisons and catalog UCAC4 r (thin yellow).

all brighter than 17.5 mag. Correcting stellar colours so that the average sky background difference across the full sample is zero in r yields corrections of 0.50, 0.00, -0.27, and -0.22 mag in g , r , i , and z filters respectively; although less of a concern in r and i data, the mean values of the resultant sample in all four filters are very close

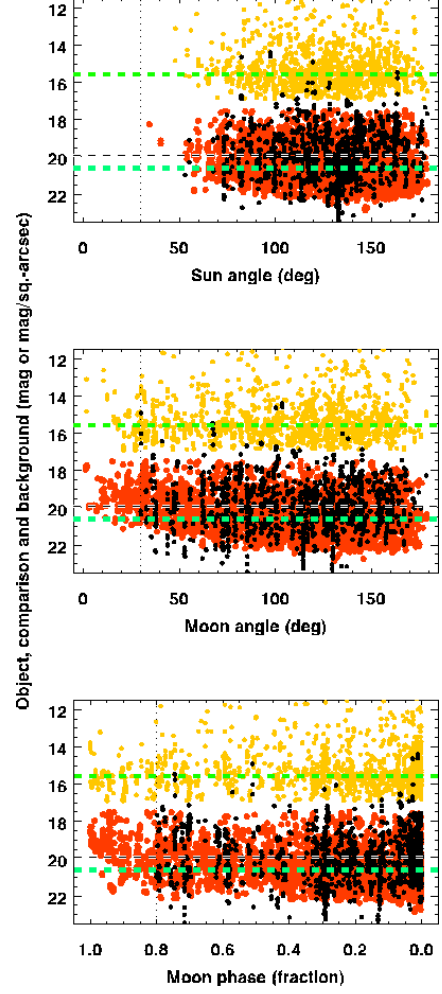


FIG. 6.— Object, comparison and sky background with angle to Sun and Moon, and Moon phase. A proximity limit of 30 degrees and 80% full Moon (horizontal dotted lines) ensure skies are suitably dark. Medians are shown as dashed horizontal lines.

to neutral (see Figure 4). The objects were also shifted by the same mean filter correction to r and uniformly taken as a differential from their catalog magnitudes. In this way, all photometry is relative to the sample average of $r = 20.0$ mag; photometry is sky-background-limited, with some down to the expected 5- σ point-source limit of about 23 mag; see Figure 5. A lower object cutoff at 21.5 mag excludes those fainter than the mean sky surface brightness, avoiding a colour bias.

The weak influence from sky brightness is illustrated in Figure 6. Only mild angle and sky-brightness restrictions were employed, with a uniform upper sky brightness cutoff of 17.5 mag arcsec⁻². To meet this, objects must have been at least 30 degrees from the Sun or Moon, and Moon phase was restricted to 80% full (see Figure 6). That this agrees well with the expectations from the linear model can be seen in Figure 7. Linear least-squares fits to extinction (comparison magnitudes), sky brightness and seeing (image quality) are shown in green (medians: dashed), giving $\alpha = 0.25$ mag, $\beta = 0.40$ mag arcsec⁻², and $\gamma = 0.38$ arcsec.

5. ANALYSIS AND RESULTS

Correlated observations were based on the sky position and UTC time recorded in each frame header. An Inter-

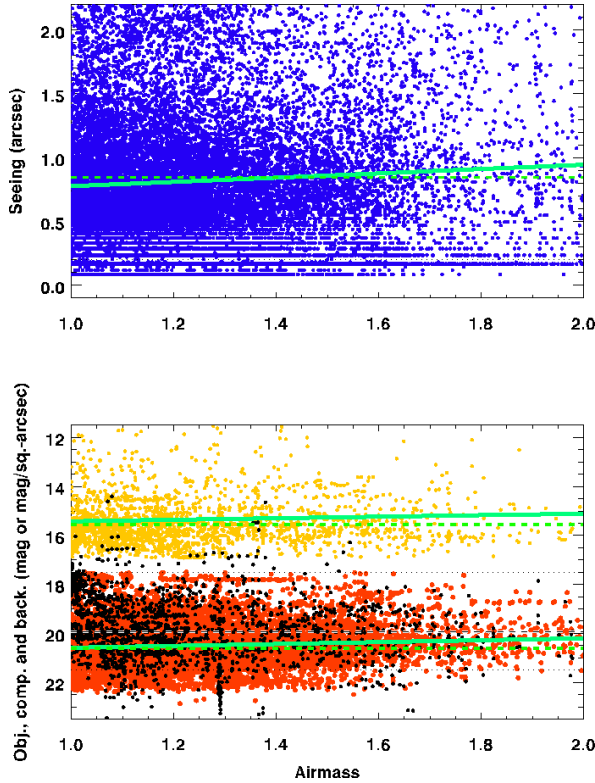


FIG. 7.— All object magnitudes obtained (filled black circles) as a function of airmass. Also shown are the UCAC4 r -band magnitudes for the comparison stars in each field (yellow) and their background sky brightnesses (red); sample limits have been applied (horizontal dotted lines). Above: image quality estimates for each frame (blue); data are spurious below a cutoff at 0.20 arcsec (horizontal dotted line).

active Data Language (IDL) code was written to perform this step, with the following prescription. For each observation, all earlier ones were searched to find those for which the end of their exposure duration overlapped by some fraction with the current one. A positive fraction means that there is some overlap. Perfect overlap, or perfect coincidence, would be a fraction of unity, and all less - down to zero - indicates that for equal fluxes this fraction of photons in the exposure would overlap with those taken in the other: over 50% is considered “coincident.” A negative fraction means that there is no overlap in the exposure durations, however, it is still useful in characterizing the temporal aspects of the sample. Observations were considered “correlated” if they fell within a given temporal window. For example, an initial check was to find if another observation occurred within the same observational “day” for the combined Gemini telescopes, which varies during the year, but is about 11 hours plus the timezone difference, or 17 hours. The largest possible window was to look back for frames within 14.5 years, to the beginning of records.

Some fully coincident observations did occur, that is, object pairs with fractional overlap of unity (310 times). One such case with multiple repeated observations is shown in Figure 8, for quasars SDSS J141624.14+134656.6 and SDSS J141632.99+135001.5, observed with GMOS-North 26 times together over the course of about month (the MJD observation times are indicated), when those two happened to fall within the same frame. In most cases, the comparison star was the

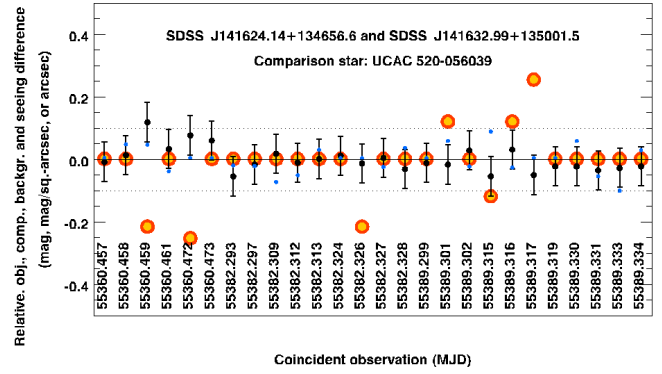


FIG. 8.— Differences in object, seeing, sky background and extinction for two particular quasars falling within the same frame, spanning about a month. These demonstrate the good data quality and photometric accuracy obtained for the sample.

same (UCAC4 520-056039) and so there is no difference in measured sky background (red circle), extinction (yellow) or seeing (blue dots). Those differ, however, in the few cases where a different calibration star was found (automatically) for the other. Spanning these observations, the uniformity of the photometry is remarkably stable. It is evident that photometry of quasars near the mean sample brightness (catalog magnitudes of 19.7 mag and 19.8 mag) was carried out over multiple observations over month-long timescales within a limit of 0.10 mag, which is considered the limit of significant measurable differences for the rest of the sample.

Several repeat, correlated observations having brightness differences larger than the significance limit are provided in Table 1, ordered by the span of observations. Only those with at least 10 occurrences are retained; uncertainties reported are standard deviations. These are, effectively, the most correlated objects in the study. They were observed from both North and South, and through the full range of catalog brightness. There are notably cases of bright (up to 17.5 mag) quasars, although none is reported in the literature as a known variable. For example, 3C 186.0 ($z = 1.07$) is a well-studied radio-loud source with a prominent jet (Chiaberge et al. 2017): observed 11 times beyond the significance limit, on average 0.40 mag less than its catalog Red magnitude (and even brighter than its SDSS r magnitude of 17.88). The largest discrepancies from the catalog are over a magnitude, occurring for fainter objects, as expected. Possibly, monitoring of targets could reveal intrinsic, intra-day brightness fluctuations. There was, however, no case of significant object difference between the two telescopes obtained within a single-day window. Even so, those observations with one object in the FoV (either North or South, but not both), are shown in Figure 9. There are some outliers, for example, occasions of particularly good seeing at low elevation. But it can be seen how expectations for intra-day variation in seeing, sky background, and extinction values - for those cases that had a comparison star suffering less than 2 magnitudes of extinction - are consistent with observations.

Full cross correlation of the entire catalog indicates no evident bias in sample selection. Figure 10 shows the ratio of redshifts of any two objects as a function of angular separation. Although the visibility of objects from the two sites necessarily results in density variation of this distribution, it is fair, with no average redshift dif-

TABLE 1
MULTIPLE SIGNIFICANT OBJECT DIFFERENCES ORDERED BY SPAN OF SAMPLES

Name	R.A. (deg)	Dec. (deg)	z	Cat. (mag)	Obj. (mag)	Diff. (mag)	n	Start (MJD)	Span (days)
SDSS J090752.02+135829.2	136.96675	13.97480	1.7	20.2	19.19 ± 0.41	-1.01	12	56040.040	0.0239
SDSS J081839.27+574750.6	124.66362	57.79739	1.632	20.6	19.85 ± 0.12	-0.75	12	55153.474	0.0241
SDSS J081838.61+580235.7	124.66088	58.04328	1.2	21.0	20.64 ± 0.07	-0.36	12	55158.523	0.0248
SDSS J120835.93+020559.4	182.14975	2.09986	2.302	20.2	20.35 ± 0.06	0.15	10	55270.223	0.0267
SDSS J120843.80+020840.8	82.18250	2.14467	1.0	19.6	20.46 ± 0.06	0.86	10	55270.223	0.0267
SDSS J111010.37+011423.8	167.54321	1.23994	0.4	22.0	20.85 ± 0.72	-1.15	14	55587.294	0.0460
SDSS J002251.40+155652.3	5.71417	15.94789	2.235	20.4	19.85 ± 0.17	-0.55	17	55774.540	0.0702
3C 186.0	116.07279	37.88811	1.068634	17.5	17.10 ± 0.11	-0.40	11	54151.217	0.1140
SDSS J042619.41+165726.8	66.58092	16.95747	0.5	20.4	18.65 ± 0.13	-1.75	30	52591.485	1.0454
2QZ J112636.9+003454	171.65408	0.58208	0.550493	17.9	18.33 ± 0.30	0.43	10	54918.397	1.0872
MC 1043-291	161.41917	-29.45722	2.128	18.9	18.45 ± 0.21	-0.45	18	53795.325	1.8113
NBCK J140849.77-010850.5	212.20737	-1.14739	2.0	21.4	20.80 ± 0.40	-0.59	29	53848.160	2.0415
SDSS J135335.92+401723.1	208.39971	40.28975	1.9	20.9	20.05 ± 0.16	-0.85	23	52701.576	2.0511
SDSS J003027.98+261804.2	7.61658	26.30119	1.534	20.1	19.88 ± 0.05	-0.22	10	55471.265	4.1237
VA-562	7.60862	26.28028	0.269	18.2	18.92 ± 0.05	0.72	22	55471.263	4.1261
SDSS J095155.67+220947.5	147.98200	22.16319	0.634413	17.9	17.67 ± 0.12	-0.23	10	55296.298	9.9686
SDSS J095205.98+221018.8	148.02492	22.17192	2.627	20.3	19.99 ± 0.12	-0.31	10	55296.298	9.9686
SDSS J141624.14+134656.6	214.10063	13.78242	2.259	19.8	20.88 ± 0.07	1.08	27	55360.457	28.8773
SDSS J141632.99+135001.5	214.13750	13.83375	1.0	19.7	19.93 ± 0.09	0.22	29	55360.457	28.8773
SDSS J023639.93+282308.2	39.16642	28.38561	1.9	21.1	20.12 ± 0.07	-0.98	12	54707.543	35.9549
SDSS J023653.25+282142.3	39.22188	28.36178	1.0	19.9	19.24 ± 0.06	-0.66	12	54707.543	35.9549
IXO 10	50.66833	-37.27778	0.515	19.5	20.04 ± 0.36	0.54	15	54760.314	308.0033
IXO 69	190.90213	11.50256	1.195	18.9	18.18 ± 0.19	-0.72	15	54180.450	682.9031
LBQS 1308-0104	197.83021	-1.34192	2.620	17.5	18.18 ± 0.20	0.68	11	52267.626	730.0214
SDSS J002235.96+001850.0	5.64983	0.31390	1.6	20.1	20.62 ± 0.27	0.52	23	52141.458	1383.9300
CXOMP J01527-1359	28.18250	-13.98361	0.821	20.9	20.46 ± 0.35	-0.44	10	52474.553	2244.6849

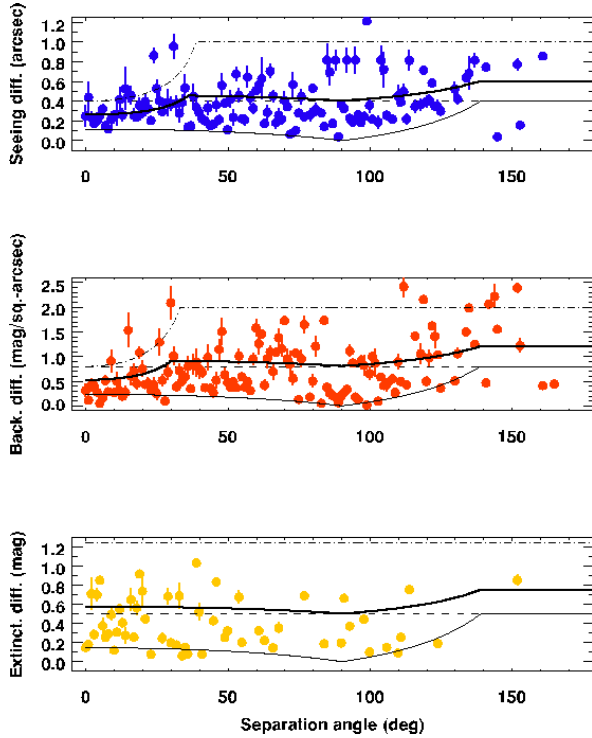


FIG. 9.— Differences in seeing, sky background and extinction occurring within a single day; a nightly window starting at twilight at Cerro Pachon and lasting approximately 17 hours. Data are averaged in 1-degree-wide bins, with 1- σ error bars.

ference across the sample (green curve). Ideally, the test sample would include only $z \geq 3.65$ objects 180° apart, but with just 274 such observations taken instead across the full sky, there was not a sufficient sample to provide a meaningful comparison of just those.

The most interesting result for the full cross-correlated

sample is that there is significant object correlation at all, even if it is not certain how that might impact a real test. Results are shown in Figure 11. Only cases where objects were within 2 magnitudes of each other and having a relative Blue-Red colour difference less than 0.20 mag were retained. These are displayed as the relative differences in the objects, averaged in 1-degree-wide bins (grey) and 6-degree-wide bins (black). The error bars are their 1- σ standard deviations. The results for just the coincident pairs are shown in light blue, that is, those cases where two objects fell within the FoV. Above are the differences for comparison stars; for reference, differences in seeing (blue) sky brightness (red), and the catalog magnitudes (green) are overplotted. These are all relatively flat (the standard deviation in comparison magnitude differences is 0.024 mag), which makes the comparison to Bell's inequality (thick black curve) remarkable. That is in better agreement than either the strict quantum-mechanical curve (thin black) or flatness (dashed), to within the deviation expected, at $S/N = 3$. It should be emphasized that this is not a fit, and all parameters were specified in Section 2 by the sample conditions. But analysis of the cumulative distribution functions do confirm a good match: the Anderson-Darling (AD) test statistic is 0.015, and it rejects the null-hypothesis of flatness at 97.7% probability ($AD = 0.886$, p-value of 0.023). Results are similar, with expectedly more scatter, if only r -band frames are used.

These deviations of differences in object brightnesses are significant relative to the measured errors; they cannot be accounted for by photometric uncertainty. A significance limit of 0.10 magnitudes is indicated by a horizontal dotted line in Figure 11. The enhancement near 60° seems secure; one near 120° less so, but still consistent with the data. The distribution of these differences is displayed as well in Figure 12. In the top panel a ver-

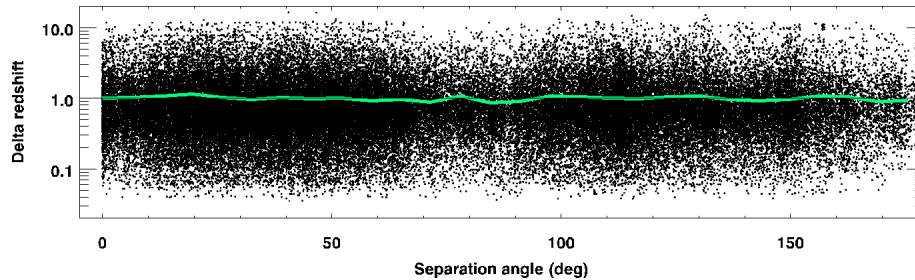


FIG. 10.— Ratios of redshifts between objects by their separation angle, for all cross-correlated observations back to the beginning of available records. Averages are in six-degree-wide bins (green) close to an expected perfect median of unity.

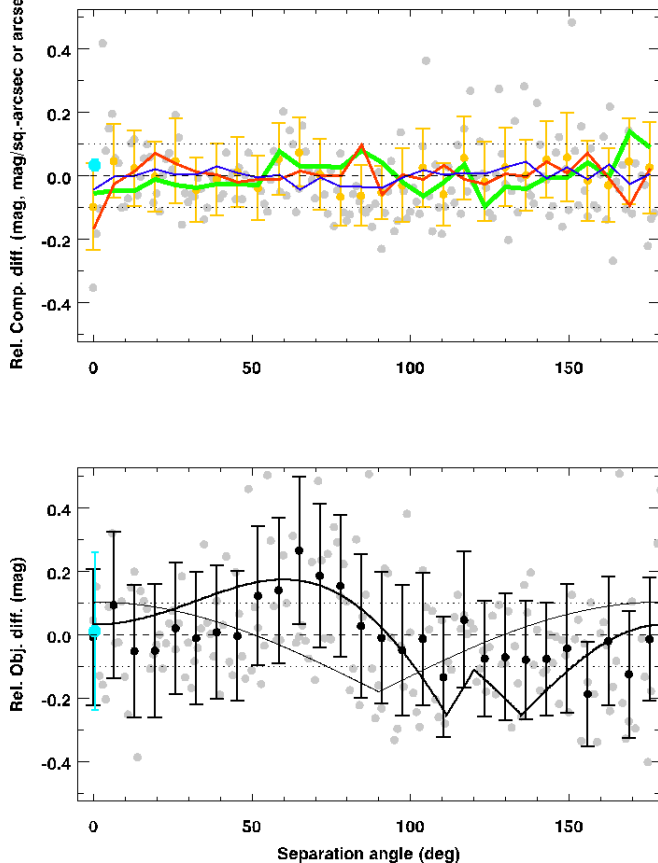


FIG. 11.— Observed object differences per angular degree (grey) and averaged in 6-degree-wide bins (black) with standard-deviation error bars. The light-blue filled circle is for the coincident cases only. Above are the same, for differences in the comparison stars (yellow); the standard deviation of cross-correlated differences is 0.024 magnitudes. Compared to scatter, the differences in catalog magnitudes are flatter (green), as are sky brightness (red) and image quality (blue). So those do not seem to explain the enhancement consistent with Bell's inequality (thick black curve).

tical dotted line shows the limit of 0.10 magnitudes; a thin black curve is a Gaussian of width 0.25 magnitudes, consistent with purely photometric error; a dashed line is the expected difference for a uniform sample of width 1.25 magnitudes. This is intuitively the limit one would expect, if the sample was randomly drawn from the same distribution, 1.00 magnitudes wide. Note the four or five instances near differences of about 0.50 magnitudes that are above this line, so occurring slightly more often than one would expect from a randomly drawn sample.

With reversed seasons between North and South hemispheres, one would expect some seasonal dependence on

when objects were observed, and so although they may be selected on the chance they appear in either telescope FoV this selection will not be uniform over the year. The bottom panel averages in 6-month-long bins those cases which were beyond the significance limit from the sample (black). The thin black curve shows the result if half the sample were selected, decaying geometrically back towards the beginning of the window. The yellow circles are the comparisons for the full sample, the green line is the same except sample times have been randomized across the entire 14.5 years. Note that this resampling has no effect on the results displayed in Figure 11; those are absolute values, so the order in which the differences were taken is not relevant, and those have already been cross correlated for the full sample. It is interesting that there appear to be some periods when it was more probable than random that there would be significant differences between two objects. The long timescales of those suggests that conducting an experiment avoiding such a bias may require repeat samples spanning years.

6. SUMMARY AND FUTURE DIRECTIONS

A clean Bell-inequality test employing quasars at large angular separations requires that the measured fluxes of objects at both far-separated telescopes are above the local noise. If not, this could hide a correlated signal. Fair, random sampling across the sky might sense that, if not photon-by-photon, at least on the timescale of minutes. By mining the full GMOS-North and GMOS-South archive, approximately 30,000 broadband g , r , i and z quasar images were found, with many repeated; the vast majority of which are merely serendipitous: targeting an unrelated object in the field. Photometry of each frame, which includes a stellar calibration for uniform data-quality selection, allows a careful analysis of the impact of source colour, variable sky conditions and airmass (sky background, extinction, and image quality) without explicit target or observer bias. Almost 10000 sufficiently deep observations for Gemini GMOS North and South, complete with a nearby unsaturated UCAC4 star, allowed photometry with a global zeropoint uncertainty of about 2% over a sample spanning 14.5 years. A “virtual test” was performed on those data, comprising roughly 2 million observational pairs, which in their aggregate have 0.25-magnitude $1\text{-}\sigma$ uncertainty within 6-degree-wide bins. This is sufficient to show a lack of flatness in relative object flux-differences with angular separation consistent with the form of Bell's inequality.

Although the Gemini sample covers the full sky and range of possible angular separations between objects, there were not sufficient $z \geq 3.65$ sources to provide a meaningful comparison restricted to those. A potentially

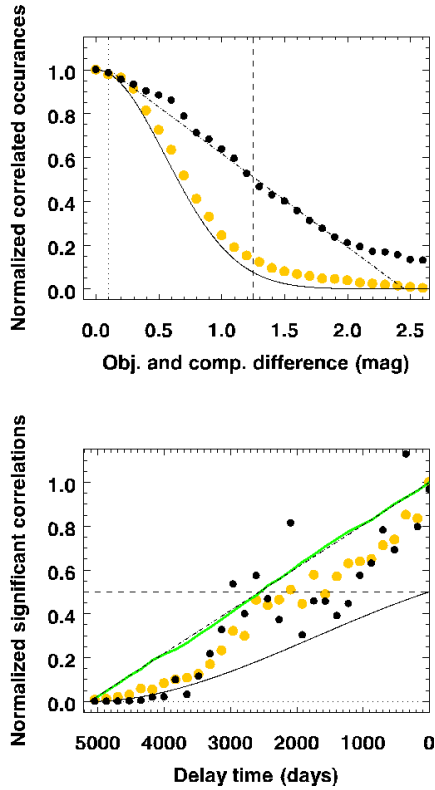


FIG. 12.— Top panel: normalized occurrences of differences between objects (black) and comparisons (yellow). Bottom panel: the same for significant differences only, as a function of delay time between correlated occurrences in days. The green line is the result when the order of data is randomized.

confusing factor may be shifting bandpasses with redshift, and correcting to a common colour; a better technique may be spectroscopic, focussed on bright emission lines. There was also limited information on how those individual sources (or the calibration stars) may have varied during this time. A subset of the data with significant differences is one output of this work, and provides a baseline from which to compare. Repeat observations of these at higher photometric precision would seem to provide a check on either real, intrinsic correlation between those source fluxes or false, spurious correlation due to unidentified source-selection or instrumental effects. Those were controlled here by the telescopes

and instruments being essentially identical, and blind selection from a prior independent catalog, but a wealth of archival sources of photometry from other telescopes could be added together to improve on this result too; multiple cross-calibration may actually serve to reduce zeropoint errors. Future facilities combined with long-term monitoring, such the Large Synoptic Survey Telescope, will make false correlation via these potential error modes much more difficult to hide.

The current dataset provides only a small number of truly coincident observations (yielding just those cases where two quasars were in the same GMOS FoV) yet that is the goal of this endeavour. Note that fair, unbiased switching in an Earth-wide QM experiment would depend on simultaneous control of local noise sources, however the discriminators are set. Practical aspects of a QM experiment and communication between sites are not dealt with here, although an attractive aspect of Gemini is that these are at two premier sites over 10600 km apart, with a combined view stretching 180 degrees across the sky. Ultimately, the coming era of 30-metre telescopes in both hemispheres is anticipated, with a D^2 aperture advantage of about $(30/8)^2 = 14$, plus a smaller PSF (and sky-background error) increasing that to $D^4 \sim 200$, bringing exposure times for $z \approx 4$ quasars down to about a second, not minutes. Thus, low-noise, truly-synchronous photometry could sample timescales (in the quasar restframe) shorter than the round-trip light travel time between telescopes, and so unambiguously exclude any collusion between measurements due to local noise. As neither the emission processes at either source nor switching-decision at either telescope could have influenced the other, the results would have to be pre-determined before the photons left the sources. In short, the experimental outcome would imply a “cosmic conspiracy” dating back nearly 90% of the look-back time for the visible Universe.

I gratefully acknowledge helpful comments on quasar QM tests by two anonymous reviewers of earlier manuscripts. This research used the facilities of the Canadian Astronomy Data Centre operated by the National Research Council of Canada with the support of the Canadian Space Agency. I thank David Bohlender in particular for his kind assistance with TAP scripts.

REFERENCES

- Einstein, A., Podolsky, B. & Rosen, N. 1935, *Physical Review*, 47, 777
- Bell, J.S. 1964, *Physics*, Vol. 1, No. 3, 195
- Chiaberge, M., Ely, J.C., Meyer, E.T., Georganopoulos, M., Marinucci, A., Bianchi, S., Tremblay, G.R., Hilbert, B., Kotyla, J.P., Capetti, A., Baum, S.A., Macchetto, F.D., Miley, G., ODea, C.P., Perlman, E.S., Sparks, W.B. & Norman, C., 2017, *A&A*, 600, 57
- Clauser, J.F., Horne, M.A., Shimony, A. & Holt, R.A. 1969, *Phys. Rev. Lett.*, 23, 880
- Friedman, A.S., Kaiser, D.I. & Gallicchio, J. 2013, *Phys. Rev. D*, 88, 044038
- Gallicchio, J., Friedman, A.S. & Kaiser, D.I. 2014, *Phys. Rev. Lett.*, 112, 110405
- Hanbury Brown, R. & Twiss, R.Q. 1956, *Nature*, 178, 1046
- Handsteiner, J., Friedman, A.S., Rauch, D., Gallicchio, J., Liu, B., Hosp, H., Kofler, J., Bricher, D., Fink, M., Leung, C., Mark, A., Hien, T., Nguyen, H.T., Sanders, I., Steinlechner, F., Ursin, R., Wengerowsky, S., Guth, A.H., Kaiser, D., Scheidl, T. & Zeilinger, A. 2017, *Phys. Rev. Lett.*, 118, 060401
- Kasten, F. 1965, A New Table and Approximation Formula for the Relative Optical Air Mass
- Li, M.-H., Wu, C., Zhang, Y. *et al.* 2018, *Appl. Phys. Lett.*, 121, 080404
- MacLeod, C.L., Ivezi, J., Kochanek, C.S., Kozłowski, S., Kelly, B., Bullock, E., Kimball, A., Sesar, B., Westman, D., Brooks, K., Gibson, R., Becker, A.C. & de Vries, W.H. 2010, *ApJ*, 721, 1014
- Mudd, D. *et al.* 2018, *ApJ*, 862, 123
- Rauch, D., Handsteiner, J., Hochrainer, A. *et al.* 2018, *Phys. Rev. Lett.*, 121, 080403
- Rosenfeld, W., Burchardt, D., Garthoff, R., Redeker, K., Ortiegel, N., Rau, M. & Weinfurter, H. 2017, *Phys. Rev. Lett.*, 119, 010402